

Metabolomic analysis reveals a common pattern of metabolic re-programming during invasion of three host plant species by *Magnaporthe grisea*

David Parker¹, Manfred Beckmann¹, Hassan Zubair¹, David P. Enot¹, Zaira Caracuel-Rios², David P. Overy¹, Stuart Snowden¹, Nicholas J. Talbot² and John Draper^{1,*}

¹Institute of Biological Environmental and Rural Sciences, Aberystwyth University, Penlais Campus, Aberystwyth, SY23 3DA, UK, and

²School of Biosciences, University of Exeter, Geoffrey Pope Building, Stocker Road, Exeter, EX4 4QD, UK

Received 27 January 2009; revised 8 April 2009; accepted 23 April 2009; published online 11 June 2009.

*For correspondence (fax +44 1970 621981; e-mail jhd@aber.ac.uk).

SUMMARY

The mechanisms by which biotrophic and hemi-biotrophic fungal pathogens simultaneously subdue plant defences and sequester host nutrients are poorly understood. Using metabolite fingerprinting, we show that *Magnaporthe grisea*, the causal agent of rice blast disease, dynamically re-programmes host metabolism during plant colonization. Identical patterns of metabolic change occurred during *M. grisea* infections in barley, rice and *Brachypodium distachyon*. Targeted metabolite profiling by GC-MS confirmed the modulation of a conserved set of metabolites. In pre-symptomatic tissues, malate and polyamines accumulated, rather than being utilized to generate defensive reactive oxygen species, and the levels of metabolites associated with amelioration of redox stress in various cellular compartments increased dramatically. The activity of NADP-malic enzyme and generation of reactive oxygen species were localized to pathogen penetration sites, and both appeared to be suppressed in compatible interactions. Early diversion of the shikimate pathway to produce quinate was observed, as well as accumulation of non-polymerized lignin precursors. These data are consistent with modulation of defensive phenylpropanoid metabolism by *M. grisea* and the inability of susceptible hosts to mount a hypersensitive reaction or produce lignified papillae (both involving reactive oxygen species) to restrict pathogen invasion. Rapid proliferation of *M. grisea* hyphae in plant tissue after 3 days was associated with accelerated nutrient acquisition and utilization by the pathogen. Conversion of photoassimilate into mannitol and glycerol for carbon sequestration and osmolyte production appear to drive hyphal growth. Taken together, our results suggest that fungal pathogens deploy a common metabolic re-programming strategy in diverse host species to suppress plant defence and colonize plant tissue.

Keywords: metabolome re-programming, host susceptible response, *Magnaporthe grisea*, *Brachypodium distachyon*, rice, barley.

INTRODUCTION

Fungal pathogens of higher plants are able to form intimate associations with host cells during biotrophic phases of disease establishment. Recent evidence suggests that invading microbes actively suppress plant immune responses in susceptible plants using proteinaceous effector molecules that can also be recognized by plant *R* gene products in incompatible interactions (Chisholm *et al.*, 2006). In addition to counteracting plant defences, a successful pathogen must also subvert host plant metabolism

in order to enable the efficient uptake, sequestration and utilization of host-derived nutrients (Solomon *et al.*, 2003; Swarbrick *et al.*, 2006; Divon and Fluhr, 2007). Several recent publications have used transcriptional profile analysis to investigate the global changes in gene expression that occur during host invasion by biotrophic and hemi-biotrophic fungi (Caldo *et al.*, 2004; Both *et al.*, 2005; Jantasuriyarat *et al.*, 2005; Doehlemann *et al.*, 2008), and have revealed co-ordinated expression of a range of gene products, with

those having a predicted metabolic function often predominant. Surprisingly, our current knowledge of metabolic interactions at the host–pathogen interface is rather limited, with the exception of the well-documented reduction in photosynthesis and re-programming of host carbon partitioning when disease symptoms are clearly visible 3–4 days after initial infection as fungal biomass is beginning to dominate the disease interaction (Chou *et al.*, 2000; Swarbrick *et al.*, 2006; Doehlemann *et al.*, 2008). Metabolic interactions allowing establishment of invading pathogens at pre-symptomatic stages of host colonization are much less well understood. Application of non-targeted, metabolomic approaches (Bino *et al.*, 2004; Catchpole *et al.*, 2005) for the study of susceptible hosts invaded by fungal pathogens may therefore provide new insight into specific aspects of metabolism associated with disease establishment in plants.

Magnaporthe grisea is the causal agent of rice blast and penetrates plant cells in a manner that is typical of a wide range of biotrophic and hemi-biotrophic cereal pathogens (Talbot, 2003; Kankanala *et al.*, 2007; Parker *et al.*, 2008). Germination of a three-celled conidium (asexual spore) on the leaf surface is followed by production of a dome-shaped appressorium cell at the end of an extended germ tube. These specialized infection structures adhere tightly to the plant surface and generate hydrostatic turgor that enables an infection peg to be pushed through the cuticle, allowing entry into the first leaf epidermal cell approximately 24 h after the spore arrives at the leaf surface (Talbot, 2003). In a susceptible host, the infection peg produces a filamentous primary hypha from which bulbous invasive hyphae soon develop, and in 36–48 h they fill the compromised epidermal cell (Talbot, 2003; Kankanala *et al.*, 2007). The initial cell remains intact and fungal hyphae are ensheathed by the invaginated plant plasmalemma (Kankanala *et al.*, 2007). Invasion of adjacent epidermal and mesophyll cells then proceeds, and may be mediated by plasmodesmata, based on the results of recent live-cell imaging studies (Kankanala *et al.*, 2007). Infected plant cells initially remain viable, and plant cell death becomes apparent only when the fungus has extensively colonized leaf tissue. Approximately 72–96 h after the initial penetration, chlorosis of the tissue and lesion formation are observed, with necrosis of infected plant tissue and sporulation of the fungus.

One of the particular challenges of metabolomic analysis is to be able to discern important changes associated with a specific biological process and clearly separate these from the biological variability and dynamic nature of metabolic changes within cells. We reasoned that one way of defining the biochemical signature associated with rice blast disease would be to use a single strain of *M. grisea* to infect three susceptible plant species, and then to determine whether a common metabolite signature is associated with the onset of blast disease. The rice blast fungus is capable of infecting a range of grass species, although individual host-limited

forms of the fungus have a much narrower host range. We utilized *M. grisea* strain Guy11, which is able to cause disease in rice (*Oryza sativa*), barley (*Hordeum vulgare*) and the model grass species *Brachypodium distachyon*. A previous metabolite fingerprinting study of non-polar chemistry (Allwood *et al.*, 2006) demonstrated differential accumulation of phospholipids between resistant and susceptible responses of two *Brachypodium distachyon* ecotypes 3 days after pathogen challenge, at which time visible lesions were evident on leaves. This complementary investigation focuses on the ability of *M. grisea* to modulate host metabolism in pre-symptomatic tissues of susceptible plants, and relies on a recently reported inoculation and sample pre-screening procedure to ensure data alignment in these dynamic host–pathogen interactions (Parker *et al.*, 2008). To produce a non-targeted overview of the metabolome, we used flow injection electrospray ionization mass spectrometry (FIE-MS) (Catchpole *et al.*, 2005; Beckmann *et al.*, 2007, 2008) to perform metabolite fingerprinting. After data modelling (Enot *et al.*, 2006, 2007, 2008; Enot and Draper, 2007), the predicted identity and relative levels of metabolites associated with disease establishment were investigated further by more targeted GC-TOF-MS profiling (Catchpole *et al.*, 2005; Beckmann *et al.*, 2007, 2008). Here we describe early changes in several host metabolic pathways that are potentially targets for pathogen-mediated perturbation of plant metabolism and suppression of host defences. We also demonstrate that re-programming of host metabolism is associated with establishment of a nutritional interface between the pathogen and host at an early pre-symptomatic stage of infection.

RESULTS AND DISCUSSION

Metabolite fingerprinting reveals dynamic changes in host plant metabolism during blast infections

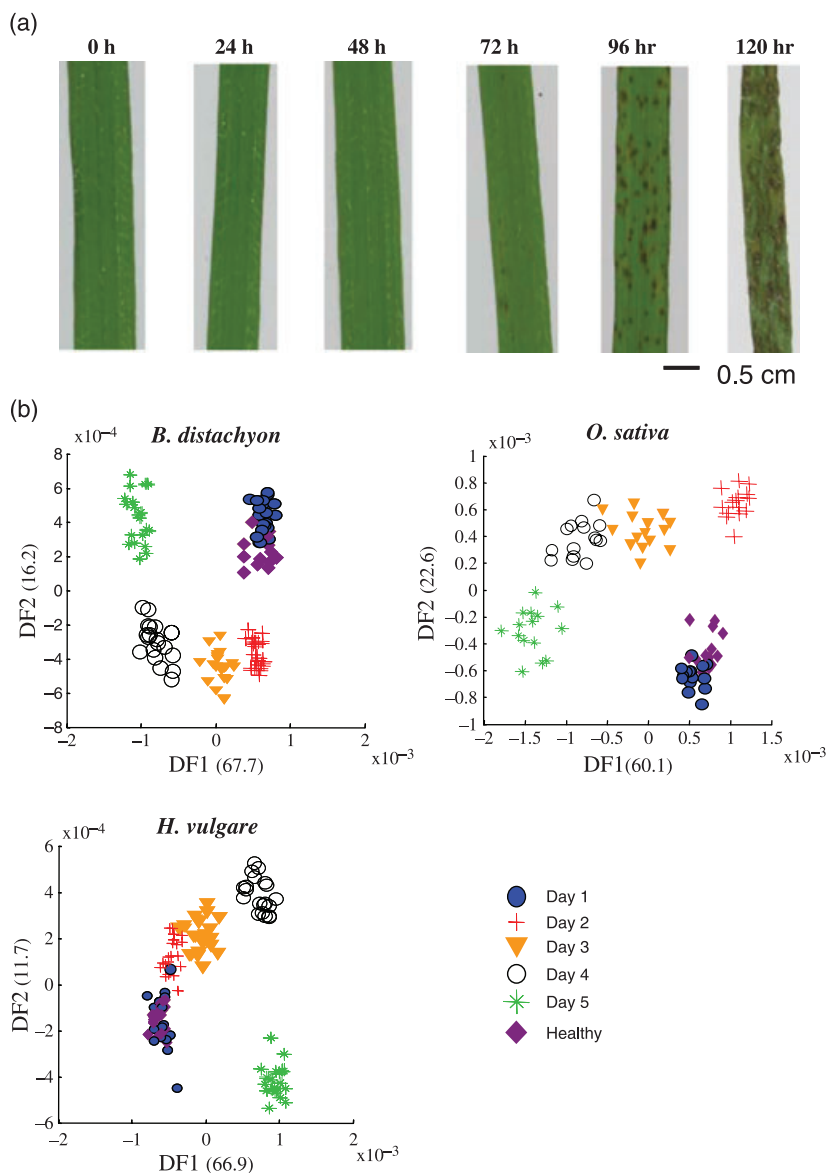
Our experimental design involved the use of three susceptible host plant species and a single strain of *M. grisea* (Guy11). Although the blast disease response in the three plant hosts occurred on slightly different time scales, epidermal penetration and the development of the fungus within the host cells were the same (Talbot, 2003; Routledge *et al.*, 2004; Parker *et al.*, 2008), and infections always culminated in a high degree of hyphal spread in plant tissue and extensive blast symptoms. The typical appearance of *M. grisea*-challenged *Brachypodium distachyon* leaves (Parker *et al.*, 2008) at various times after infection is shown in Figure 1(a). We wished to detect any subtle effects of the pathogen on plant metabolism in pre-symptomatic tissue, and thus all metabolite fingerprint data sets were validated rigorously before subjecting to data analysis (see Figure S1).

Supervised data analysis techniques such as linear discriminant analysis (LDA) are used to build models that

Figure 1. Monitoring metabolome changes during invasion of three susceptible hosts by *M. grisea* strain Guy11 using FIE-MS fingerprinting.

(a) Development of typical disease symptoms in leaves of *B. distachyon* ABR1 over a 5-day period.

(b) Score plots of a linear discriminant analysis of FIE-MS fingerprint data representing infected leaf samples taken at five time points after infection of *B. distachyon*, *O. sativa* and *H. vulgare*. The numbers in parentheses indicate the percentage of overall variance contained in the first two discriminant functions (DF).



discriminate between labelled data (Enot *et al.*, 2006, 2007, 2008; Enot and Draper, 2007). An LDA scores plot is a useful way of visualizing the relationship between sample classes; any samples that are difficult to discriminate will group very closely in such plots and may be considered to be very similar. Validated FIE-MS fingerprint datasets representing each of the three infected host species were thus subjected to LDA to determine whether distinct metabolome changes were associated with disease progression. Figure 1(b) illustrates a typical result using positive ion data (100–2000 *m/z*), but similar observations were made using negative ion mode (data not shown). Samples within each individual class clustered tightly, but little discrimination was observed between healthy controls and tissues harvested 24 h after infection. However, samples representing later time points in disease progression were generally well separated.

Data model feature selection identifies clusters of infection phase-specific fingerprint signals common to three host species

Although LDA efficiently highlighted phases of the infection process at which major changes in the metabolome occurred, such techniques cannot determine easily which 'explanatory' data features (i.e. FIE-MS *m/z* signals) are responsible for sample discrimination. We have shown previously that the random forest (RF) decision tree algorithm has many useful properties for modelling metabolite fingerprint data and is capable of ranking features for importance in classification models (Enot *et al.*, 2006, 2007, 2008). The numbers of *m/z* signals ranked highly by RF within positive ion data corresponding to various *P* value thresholds are shown in Table S1. At a *P* value of

approximately 0.0025, the explanatory signals showed a step increase in number in all three host species, and therefore this *P* value was chosen as a nominal significance threshold to identify potentially 'explanatory' signals for further analysis.

A preliminary visual examination of the lists of significant signals in both positive and negative ion data suggested that a large proportion of the highly ranked *m/z* signals within each phase of disease establishment were common to all three host–pathogen systems. These highlighted signals were subjected to MS/MS^{*n*} analysis (Overy *et al.*, 2008) to confirm whether they represented the same metabolite at each time point in all three compatible host–pathogen interactions (Figure 2a,b). In total, 69 discriminatory positive ion signals and 33 significant negative ion signals (excluding isotopes) were found to be common to *B. distachyon*, *H. vulgare* and *O. sativa* leaves challenged with *M. grisea* strain Guy11. The explanatory signals in positive ion data from a typical susceptible interaction (*B. distachyon*) are illustrated in Figure 3, and are aligned in ascending mass order as indicated on the left of the figure (see also Figure S2 for negative ion data). Figure 3 also highlights the fact that no variables were discriminatory across all infection time points, indicating that the individual phases of disease progression feature a dynamically changing metabolome.

Metabolite identity predictions from FIE-MS and GC-TOF-MS analysis suggest common alterations in many areas of host metabolism during distinct phases of disease progression

The list of highlighted metabolite signals in each ionization mode was interrogated by ARMeC, a metabolite identity prediction tool for use with nominal FIE-MS data (Beckmann *et al.*, 2007; Overy *et al.*, 2008). ARMeC can be used to generate combinations of signals that potentially represent isotopes, adducts and fragments derived from ionization of specific metabolites. In many instances, an overlapping range of metabolites had predicted ionization products that could be mathematically matched to each *m/z* (Figures 3 and S2). Where ion intensities allowed, further accurate mass measurements were made using an FT-ICR-MS detector to confirm the predictions (Tables S2 and S3). As illustrated on the right of Figure 3, the predicted metabolites are associated with a small number of distinct areas of metabolism, the most predominant of which involved carbohydrate metabolism (including mono- and disaccharide metabolism, the TCA cycle and sugar alcohol synthesis), aromatic metabolism (including synthesis of aromatic amino acids, phenylpropanoids and lignin/suberin precursors), urea cycle/proline metabolism, and fatty acid metabolism. Full lists of putative signal annotations are given in Tables S2 and S3. These data complement observations from a previous study (limited to non-polar chemistry) that reported differential accumulation of phospholipids in *B. distachyon*

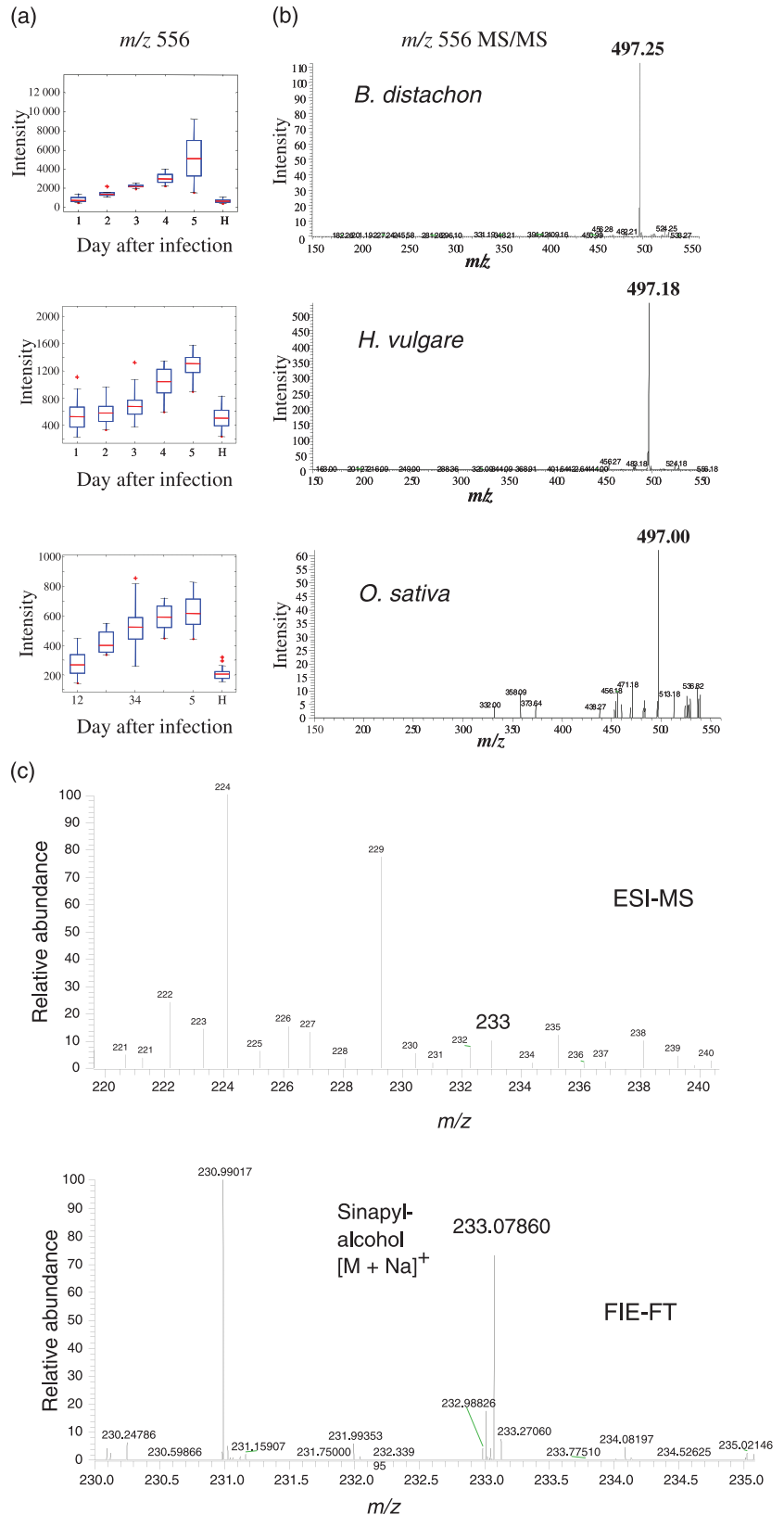
interactions with rice blast, but was not able to provide insight to areas of metabolism dominated by polar chemistry (Allwood *et al.*, 2006). A more recent study involving targeted metabolite analysis found significant increases in aromatic amino acids, shikimate and hydroxycinnamic acid derivatives and hexoses 4 days after infection in a biotrophic interaction between *Ustilago maydis* and a susceptible maize variety (Doehlemann *et al.*, 2008).

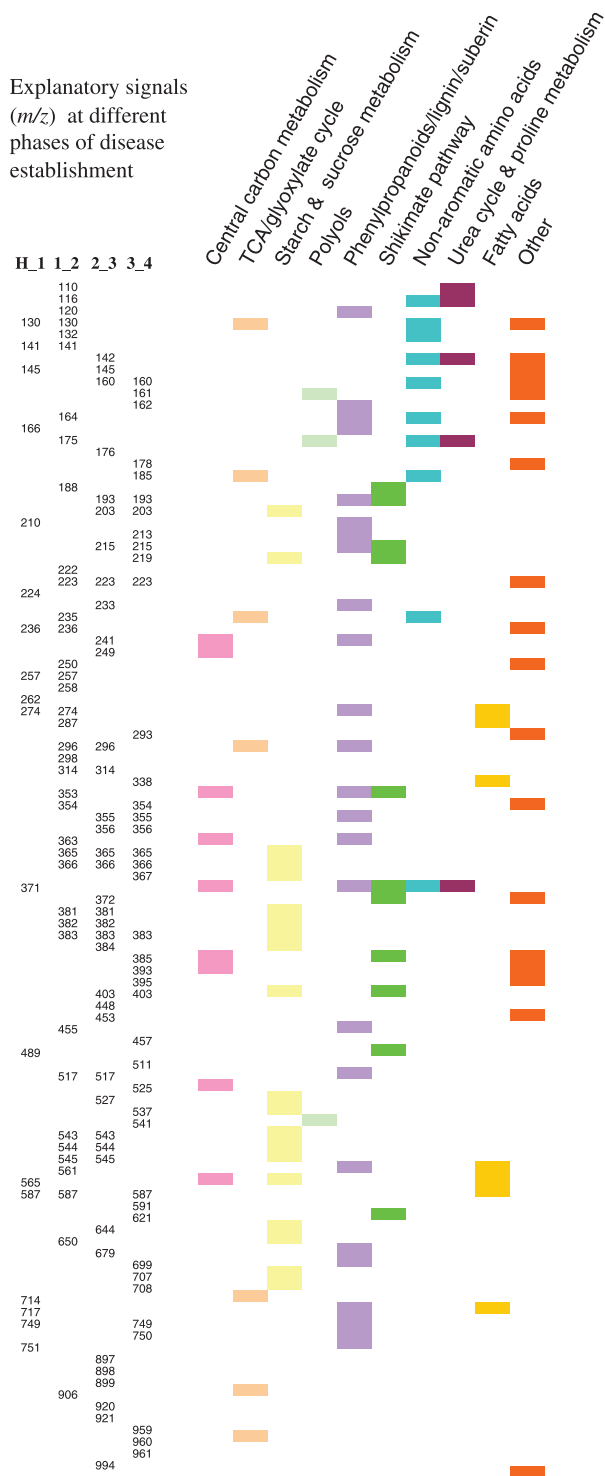
Many classes of metabolites predicted by FIE-MS fingerprinting were good candidates for analysis by GC-MS. Peaks identified in representative GC-TOF-MS chromatograms developed from *B. distachyon* samples were subjected to manual alignment to produce a peak list representative of metabolites found in each phase of disease progression. This 'master list' was used for targeted peak alignment in chromatograms derived from GC-TOF-MS profiling in all three host species (see Figure S3). Many of the peaks (approximately 48%) were positively identified using a combination of spectrum matches to the National Institute of Standards and Technology library and available standards, but many remain unknown (see Figure S4). Many of the structurally characterized GC-TOF-MS peaks represented potentially discriminatory metabolites predicted previously from the high-throughput FIE-MS analysis (Tables S2 and S3). The intensity values of these peaks were thus subjected to analysis of variance (ANOVA), and box plots representing metabolite changes in *Brachypodium distachyon* are illustrated in Figures 4 and 5, which summarize the major metabolic changes occurring during disease establishment. With the exception of tyrosine, all positively identified metabolites shown by GC-TOF-MS to be significantly altered during pathogen invasion increased over time (Figures 4a and 5a). Conserved changes in metabolite concentrations were also evident from GC-TOF-MS analysis of rice and barley infections (Figure S5).

Metabolic re-programming occurs early in pre-symptomatic leaf tissue

In resistant host plant genotypes, *M. grisea* invasion normally stops within 48 h as a consequence of localized plant defences, including production of reactive oxygen species (ROS), localized synthesis of defensive cell-wall thickenings (papillae) that restrict the availability of water and nutrients to the invading microbe (Huckelhoven, 2007), and induction of a hypersensitive response (Talbot, 2003; Routledge *et al.*, 2004; Allwood *et al.*, 2006; Parker *et al.*, 2008). Metabolite fingerprinting by FIE-MS and metabolite profiling by GC-TOF-MS in the present analysis revealed major changes in metabolome over the first 48 h in *M. grisea*-challenged leaves of all three susceptible host species. Although the effects of biotrophic/hemi-biotrophic fungal pathogens on host plant metabolism have been investigated previously (Chou *et al.*, 2000; Allwood *et al.*, 2006; Swarbrick *et al.*, 2006; Sutton *et al.*, 2007; Doehlemann *et al.*, 2008), these

Figure 2. Signal alignment and annotation in FIE-MS positive ion metabolite fingerprint data. (a) Box plots derived from ANOVA of the m/z 556 signal (positive ion mode) in FIE-MS fingerprints in samples representing a time course of the response of three grass species to infection with *M. grisea*. It can be seen clearly that m/z 556 exhibits an identical pattern of signal intensity behaviour in all three host-pathogen interactions. (b) Further evidence that the extracted ion at m/z 556 represents the same metabolite in all three species is provided by the fact that each produces an identical daughter ion of m/z 497 in MS/MS experiments using the LTQ linear ion trap. (c) The nominal mass signal at m/z 233 (top panel) was revealed to correspond to a sinapyl alcohol salt adduct (m/z 233.07860) by accurate mass measurement using an FT-ICR-MS detector.





studies were mostly limited to post-symptomatic tissues, 72 h after initial challenge. The present data show that a sophisticated re-programming of host metabolism occurs in pre-symptomatic tissues when the pathogen is still in the process of penetrating individual epidermal cells, consistent with recent transcriptome studies using barley infected with

Figure 3. Predicted areas of metabolism that alter during disease establishment in *B. distachyon* as suggested by FIE-MS fingerprinting (positive ion data).

Models derived from pairwise comparisons of FIE-MS fingerprint data representing leaf samples taken on consecutive days of the invasion process were subjected to feature selection using the random forest (RF) decision tree algorithm. The left of the figure shows the m/z (aligned in ascending mass order) that change significantly ($P \leq 0.001$) at each phase. H, healthy leaves; 1–4, days after infection. The right of the figure groups the 'explanatory' FIE-MS signals annotated by ARMeC into discrete areas of metabolism (metabolite details are given in Table S2).

Blumeria graminis (Caldo *et al.*, 2004; Both *et al.*, 2005) and maize infected by *Ustilago maydis* (Doehlemann *et al.*, 2008). In view of the exceedingly small contribution of fungal hyphae to overall biomass at this time, it is likely that the majority of extracted metabolites are of plant origin until day 3. Because rice and *Brachypodium* represent evolutionarily distant genera in the Gramineae (Draper *et al.*, 2001), these data may provide evidence for conserved pathogen targets that perturb metabolism in both temperate and tropical grass species. A large number of metabolites increased rapidly in concentration after 72 h when lesions first appear and pathogen biomass is increased, suggesting that fungal metabolism begins to make a major contribution to overall metabolome changes only at this stage of infection.

The shikimate pathway and defensive lignification may be modified in susceptible interactions

Early defensive activation of the phenylpropanoid pathway leads to production of both anti-microbial secondary metabolites and lignin/suberin precursors for cell-wall strengthening in resistance responses (Kawasaki *et al.*, 2006; Huckelhoven, 2007). Hydrogen peroxide is required for the oxidative cross-linking of precursors during localized inducible biosynthesis of lignin and suberin polymers, which provide physical barriers to pathogen ingress, for example in production of papillae (Huckelhoven, 2007). It is notable that almost 40% of the 'explanatory' m/z are predicted to be ionization products of a wide range of defence-induced phenylpropanoid pathway metabolites, including lignin intermediates and other compounds derived from lignin precursors (Tables S2 and S3). The apparent accumulation of such metabolites may simply be a product of phenylpropanoid pathway activation or could result from poor mono-lignan polymerization in the absence of sufficient ROS. This situation may occur if activation of the phenylpropanoid pathway is delayed or defensive ROS induction is delayed/suppressed. These observations are consistent with the reported absence of primary cell-wall thickening (papillae formation) at sites of attempted fungal penetration in compatible hosts of *M. grisea* (Huckelhoven, 2007), and with the increase in free hydroxycinnamic acids found in maize leaves infected by *Ustilago maydis* (Doehlemann *et al.*, 2008).

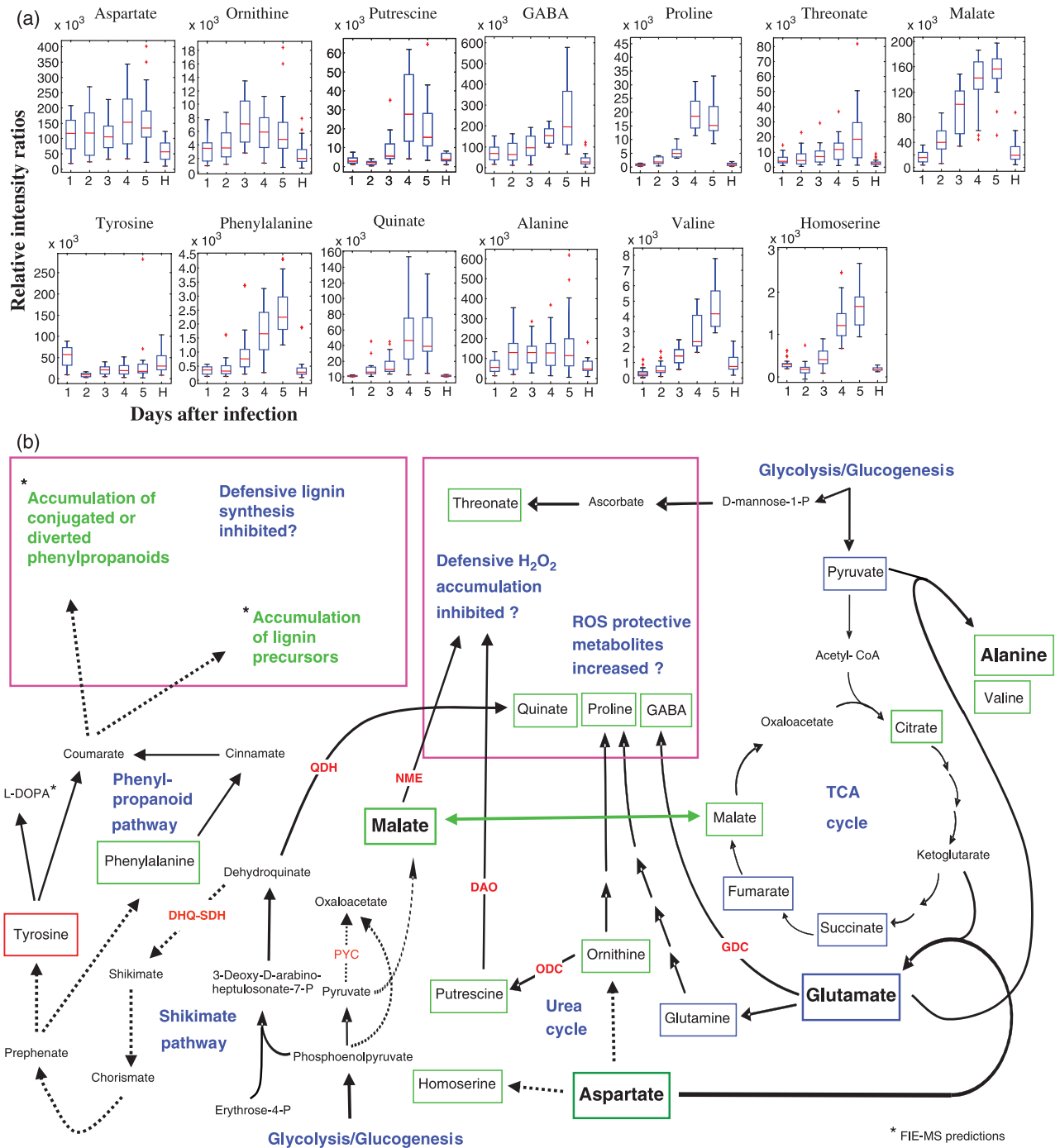
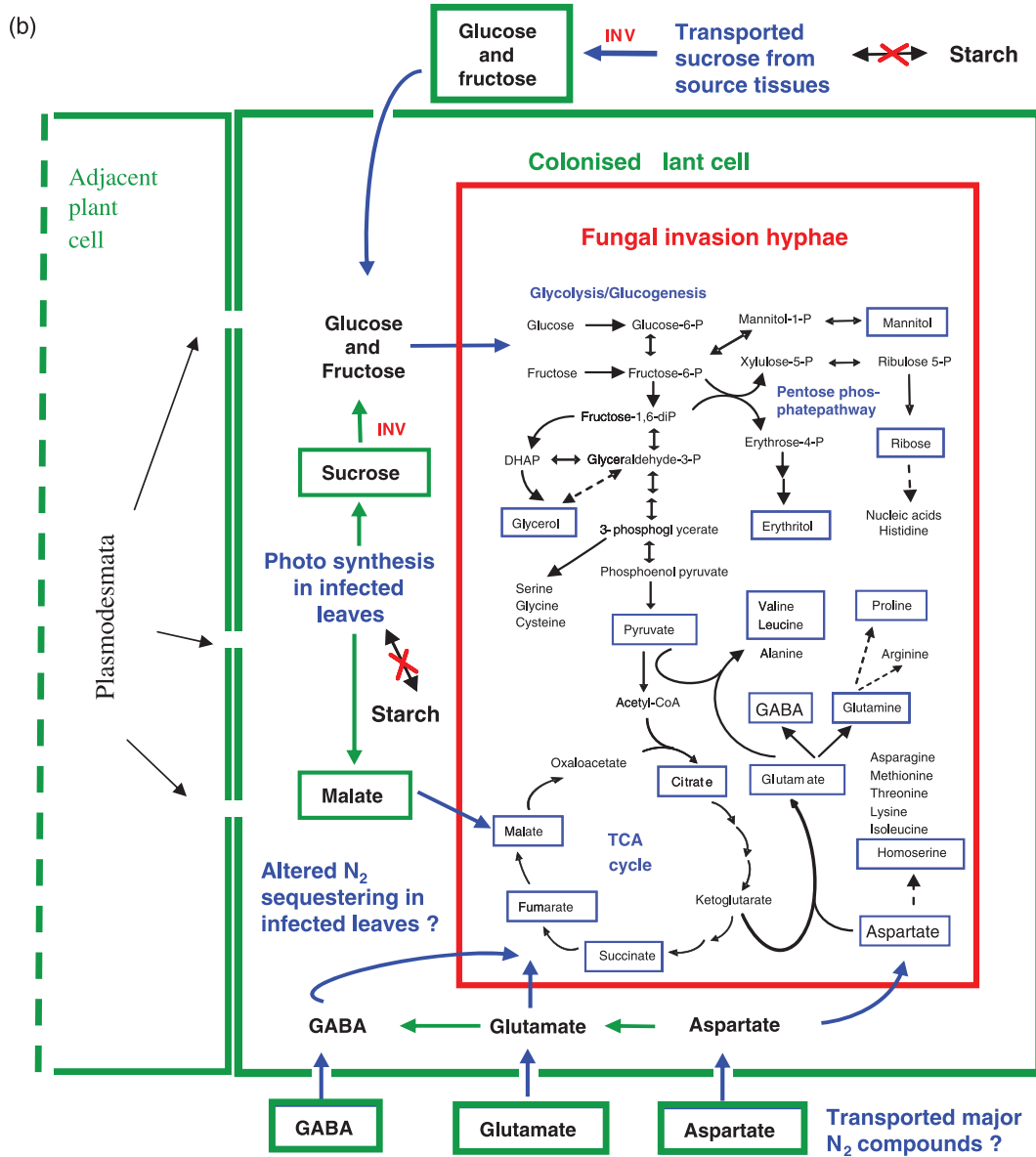
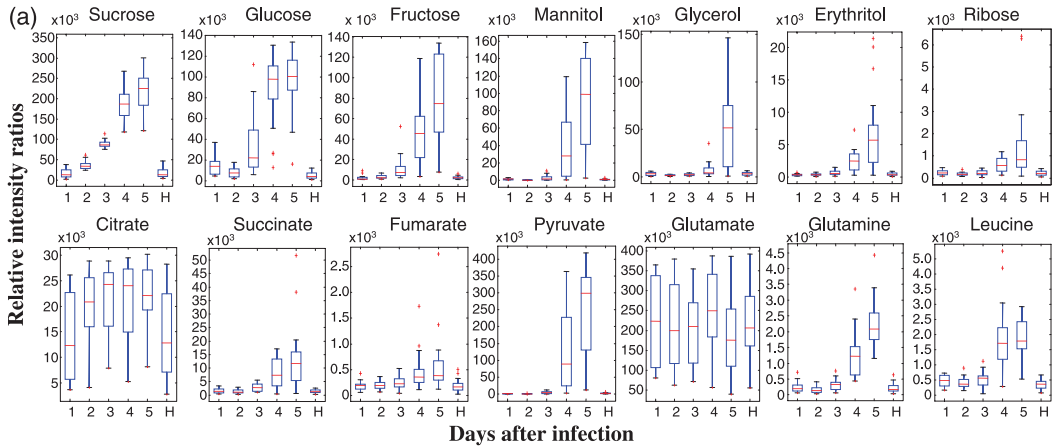


Figure 4. Metabolome changes associated with induced plant defence responses.

(a) Box plots derived from ANOVA showing changes in metabolite levels during the invasion process. H, healthy leaf; the red line indicates the median, the blue box shows the interquartile range (IQR), and bars indicate data points below the first and above the third quartile, with red crosses as individual outliers ($>1.5 \times$ IQR). (b) Model summarizing key plant metabolome changes in early phases of fungal invasion. Host enzyme activities that are potentially affected by fungal invasion are shown in red: QHD, quinate dehydrogenase; PYC, pyruvate carboxylase; NME, NADP-malic enzyme; DAO, diamine oxidase; ODC, ornithine decarboxylase; GDC, glutamate decarboxylase; DHQ-SDH, dehydroquinase dehydratase–shikimate dehydrogenase. Metabolites in blue boxes are maintained at high levels, and show only modest increases by day 3. Metabolites in green boxes show substantial increases by day 3. Metabolites in red boxes show decreased concentrations by day 3. The larger the font, the higher the metabolite concentration. Dotted arrows indicate either multiple enzymic steps or several enzymes able to catalyse the same reaction.



Phenylpropanoids are produced from precursors derived from the shikimic acid pathway (Figure 4b), which is transcriptionally activated by pathogen attack (Caldo *et al.*, 2004). An early and sustained increase in quinate, which was observed in all three host–fungal interactions, almost certainly represents a modulation of the shikimate pathway. Dehydroquinate dehydratase–shikimate dehydrogenase (DHQ–SDH) is a bi-functional enzyme in plants (Herrmann and Weaver, 1999; Singh and Christendat, 2006). Substrate channelling from DHQ to SDH active sites normally ensures a constant flux through the shikimate pathways for chorismate synthesis. If this channelling is blocked, however, then the two substrates (dehydroquinate and dehydroshikimate) become available for quinate synthesis (Singh and Christendat, 2006). Any diversion of DHQ to quinate may suppress chorismate production, and could be responsible for a delay or reduction in defensive phenylpropanoid metabolism as commonly reported in susceptible hosts upon pathogen attack.

Pathogen-mediated perturbation of host metabolism may modify the generation of defence-related ROS

Reactive oxygen species (ROS), such as H₂O₂, are important signalling molecules that are responsible for triggering the hypersensitive response in resistant interactions between host plants and potential pathogens (Allan and Fluhr, 1997; Chisholm *et al.*, 2006; Torres *et al.*, 2006). In the present study, we predicted that suppression or delay of ROS synthesis in parallel with accumulation of metabolites protective against ROS is also a dominant feature of the metabolome changes occurring during pre-symptomatic phases of disease establishment in susceptible interactions between *M. grisea* and its hosts. The network of proposed metabolome changes (Figures 4 and 5) involved several major pathways (TCA cycle, amino acid metabolism, urea cycle, glycolysis/glucogenesis, shikimate pathway and phenylpropanoid metabolism), and thus modulation of ROS-related metabolism was investigated further, starting with spatial and temporal analysis of ROS induction at sites of attempted host penetration.

Viewing of the *Brachypodium distachyon* leaf surface under epifluorescence illumination (Figure 6a) shows epidermal cells organized in files (Figure 6b) containing either trichomes or stomata (an example of each is circled in Figure 6a). This regular structure means that it is easy to count the number of individual cells producing ROS around sites of attempted pathogen invasion under DAB (3,3-

diaminobenzidine-tetrahydrochloride) staining. A simple relative staining scale was developed, dependent on the number of cells involved, staining intensity and the presence of dark, granular cytoplasm in underlying mesophyll cells (see Figure S6 for grading guide). Observation of relative DAB staining at pre-symptomatic time points after infection (Table 1) in a susceptible host (ABR1; Figure 6c,e) and a resistant host (ABR5; Figure 6d,f) revealed that ROS production encompassed a larger number of cells, was more intense and more often extended to one or two underlying mesophyll cells at sites of attempted pathogen ingress in ABR5. *M. grisea* generates ROS within the appressorium during plant infection, but this is restricted to the infection cell and does not diffuse into the surrounding environment (Egan *et al.*, 2007). The DAB staining is therefore detecting ROS generated by the host plant during challenge by the fungal pathogen. A detailed examination of cellular penetration by fungal hyphae using KOH/aniline blue staining revealed rapid growth of fungal biomass in ABR1 over the first 96 h (Figure 6g,i,k). Conversely, the pathogen was generally contained within the initial invaded cell, and adjacent cells showed extensive cytoplasm granulation in the resistant ecotype over the same time period (Figure 5h,j,l).

NADP-malic enzyme (NADP-ME) is rapidly induced by stimuli associated with plant defence (Schaaf *et al.*, 1995; Casati *et al.*, 1999), and catabolizes malate, generating NADPH that can be used as a substrate by NADPH oxidase in generation of superoxides and consequently defensive H₂O₂ (Torres *et al.*, 2006). Malate levels showed a modest increase in the resistant ecotype ABR5 but rose dramatically in the susceptible ecotype ABR1 (Figure 7a), which may be accounted for by anaplerotic synthesis directly from phosphoenol pyruvate (PEP) derived from photosynthesis in infected leaves (Figure 4b). Using an *in planta* staining method, it is clear that NADP-ME is activated at sites local to pathogen invasion (Figure 7b). More detailed observation revealed that NADP-ME activity was found only in living cells adjacent to those recently colonized by fungal hyphae (Figure S7) close to cells exhibiting strong ROS production. NADP-ME is induced in both susceptible (ABR1) and resistant (ABR5) responses (Figure 7c); staining levels were generally comparable in both ecotypes for the first 4 days after infection despite considerable differences in the number of cells penetrated by the pathogen. However, enzyme activity increased more quickly and to higher levels in ABR5 when assayed in leaf extracts (Figure 7d), particularly when

Figure 5. Metabolome changes associated with central carbon and nitrogen partitioning in infected plants.

(a) Box plots derived from ANOVA showing changes in metabolite levels during the invasion process. H, healthy leaf; the red line indicates the median, the blue box shows the interquartile range (IQR), and bars indicate data points below the first and above the third quartile, with red crosses as individual outliers ($>1.5 \times \text{IQR}$). (b) Model summarizing fungal metabolic interactions with colonized host. INV, invertase. Metabolites in blue boxes are fungal metabolites that are predicted to increase after 3 days. Metabolites in green boxes are major central carbon and nitrogen compounds that are likely to be derived from the host. The larger the font, the higher the metabolite concentration. Blue arrows indicate transport across cell walls. Dotted arrows indicate multiple enzymic steps.

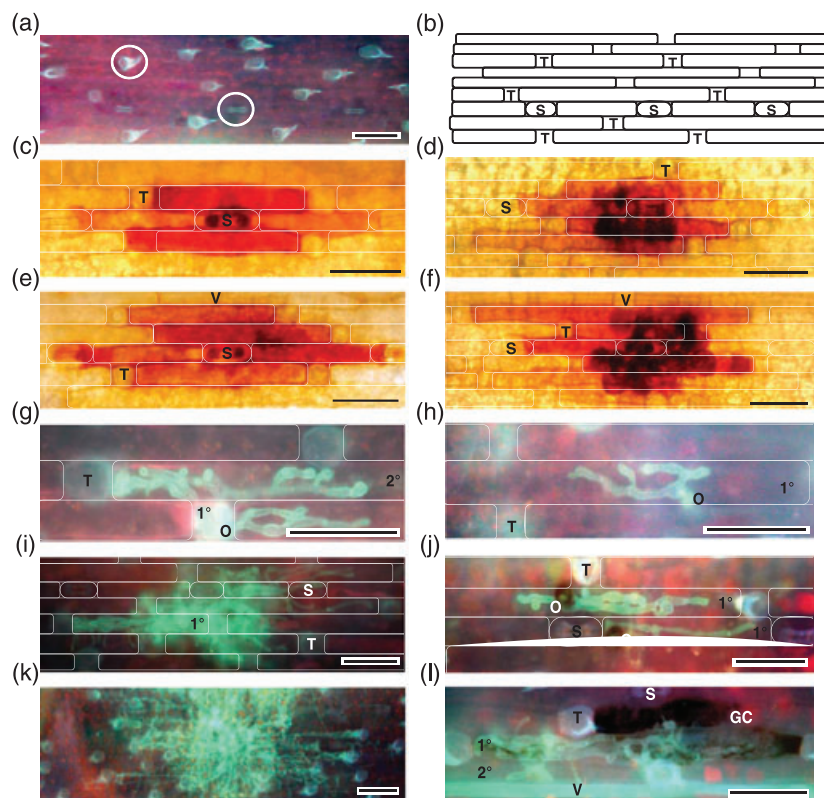


Figure 6. Host cell invasion and production of reactive oxygen species (ROS) in susceptible (ABR1) and resistant (ABR5) *B. distachyon* ecotypes infected by *M. grisea*.

(a) Part of the leaf surface of *B. distachyon* under epifluorescence showing cells organized in files containing either trichomes or stomata (an example of each is circled).

(b) Line drawing of cell boundaries in the leaf segment shown in (a).

(c–f) ROS production at sites of epidermal penetration visualized using DAB staining; cell boundaries are superimposed in white. (c) ABR1 24 h post-infection; (d) ABR5 24 h post-infection; (e) ABR1 48 h post-infection; (f) ABR5 48 h post-infection.

(g–l) KOH/aniline blue staining of fungal hyphae in *B. distachyon* leaves infected by *M. grisea* observed under epifluorescence. (g, i, k) Susceptible *B. distachyon* ecotype (ABR1); (h, j, l) resistant *Brachypodium* ecotype (ABR5); (g, h) 48 h post-infection; (i, j) 72 h post-infection; (k, l) 96 h post-infection.

T, trichome; S, stomata; V, vascular tissue; O, site of penetration; 1°, primary infected epidermal cell; 2°, secondary infected epidermal cell; GC, granulated cytoplasm.

Scale bars = 0.05 mm (50 μ m).

Table 1 Comparison of ROS production as monitored by DAB staining (see Figure S6 for a description of the scale) in early phases of susceptible (ABR1) and resistant (ABR5) interactions between *B. distachyon* and *M. grisea*

Relative staining grades	Percentage of infection sites in each relative staining grade (mean \pm SD)							
	ABR1				ABR5			
	8 h	12 h	24 h	48 h	8 h	12 h	24 h	48 h
1	92.15 \pm 0.68	37.36 \pm 2.16	13.10 \pm 3.88	3.34 \pm 1.00	64.39 \pm 1.33	26.09 \pm 0.87	8.47 \pm 2.48	2.70 \pm 1.60
2	7.85 \pm 0.68	53.30 \pm 0.36	37.24 \pm 4.55	7.43 \pm 2.24	27.80 \pm 1.43	52.17 \pm 1.34	15.25 \pm 0.05	5.86 \pm 3.19
3	–	9.34 \pm 1.80	26.21 \pm 1.61	6.32 \pm 1.94	7.81 \pm 2.77	16.30 \pm 0.03	27.12 \pm 4.72	8.11 \pm 2.54
4	–	–	12.41 \pm 0.86	12.64 \pm 0.94	–	5.44 \pm 0.50	22.04 \pm 1.17	14.64 \pm 3.75
5	–	–	8.97 \pm 4.11	11.90 \pm 3.38	–	–	14.69 \pm 3.18	17.34 \pm 2.01
6	–	–	2.07 \pm 0.75	8.18 \pm 2.34	–	–	9.04 \pm 1.90	25.90 \pm 4.97
A	–	–	–	22.68 \pm 4.77	–	–	2.82 \pm 0.86	5.40 \pm 1.32
B	–	–	–	27.51 \pm 6.39	–	–	0.57 \pm 0.23	20.05 \pm 5.81

expressed in relation to the number of pathogen-penetrated leaf cells (Figure 7e). NADP-ME activity was further assessed by an in-gel staining assay after fractionation of leaf proteins

by native PAGE (Figure 7f). NADP-ME activity was evident in three protein bands, only one of which (band 3) increased in both ABR1 and ABR5 leaves after challenge with *M. grisea*.

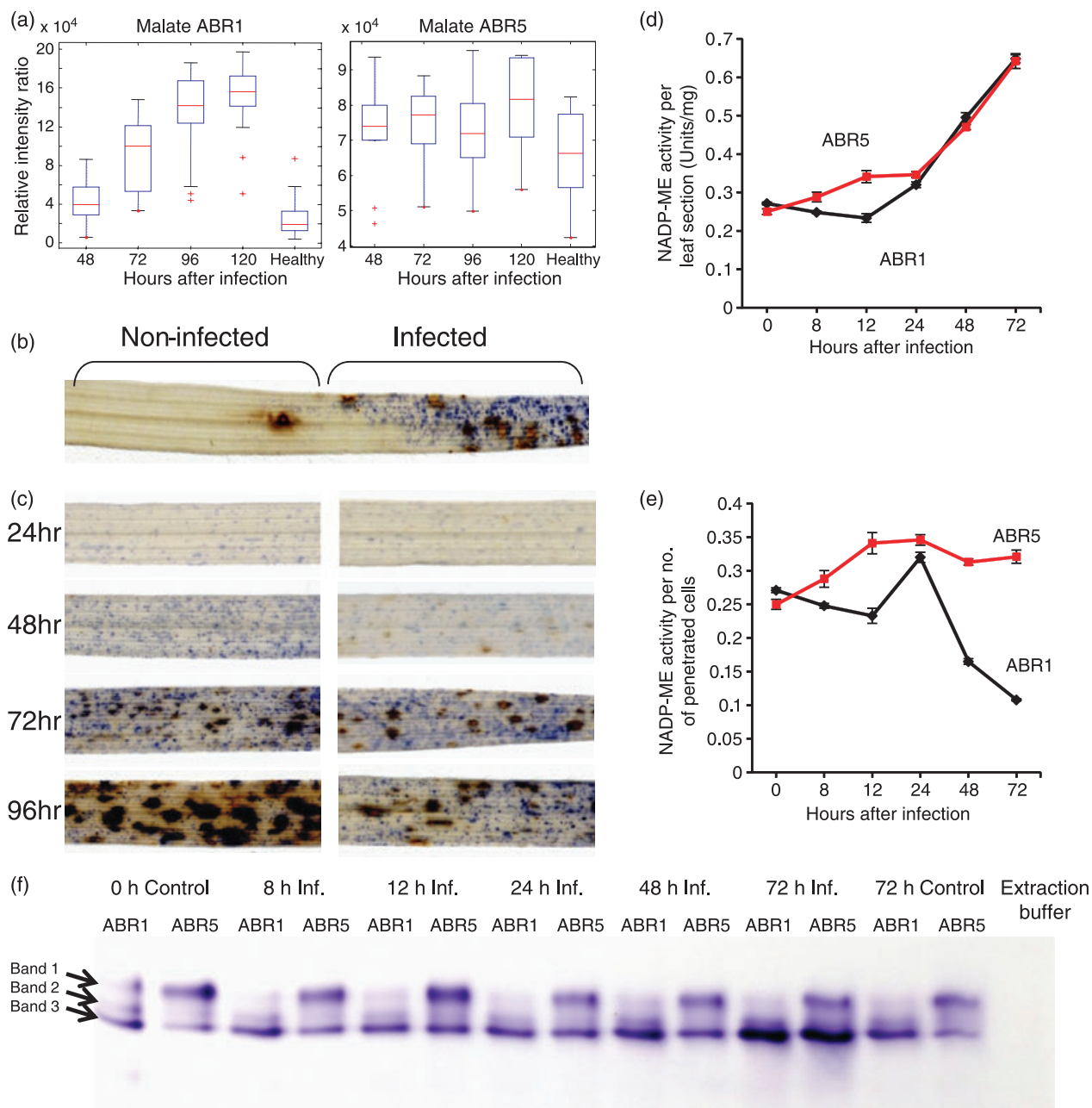


Figure 7. NADP malic enzyme activity in susceptible (ABR1) and resistant (ABR5) *B. distachyon* ecotypes infected by *M. grisea*.

(a) Changes in malate concentration (by GC-MS) with time after infection of ABR1 and ABR5 with *M. grisea*.

(b) *In situ* staining of NADP-ME activity (blue colour) associated with the infected half of an ABR1 leaf 96 h after challenge with *M. grisea*.

(c) Comparison of *in situ* NADP-ME activity in 2.5 cm sections of fully expanded leaves of ABR1 and ABR5 at various time points after infection with *M. grisea*.

(d, e) Time course of NADP-ME enzyme activity in crude extracts of two *B. distachyon* ecotypes infected by *M. grisea*. (d) Data expressed as activity per 4 cm leaf section. (e) Data expressed as activity per number of penetrated cells.

(f) Native PAGE NADP-ME in-gel activity assay using extracts from healthy and infected ABR1 and ABR5 leaves at various time points after challenge with *M. grisea*.

In parallel experiments, we demonstrated that susceptible rice varieties exhibit an increase in NADP-ME transcript abundance as leaf colonization progresses, whereas transcript levels remain stable in a resistant variety (Figure S8). These data suggest that NADP-ME is induced in cells local to sites of attempted pathogen ingress during the first 48 h of

the invasion process. Although the pathogen quickly colonizes increasing numbers of host cells thereafter in the susceptible ecotype (ABR1), the amount of NADP-ME does not show a proportional increase in activity. Such observations are consistent with malate being an important source of NADPH for defensive ROS production in grasses,

and suggest that NADP-ME activity (but not transcription or translation) may be suppressed in cells immediately adjacent to sites of host penetration in susceptible responses.

The early increase in ornithine and gradual accumulation of putrescine (Figure 4a) suggest that defensive H₂O₂ production via the action of diamine oxidases (Walters, 2003; Yoda *et al.*, 2003) may be inhibited in susceptible interactions (Figure 4b). Accumulation of substrates that indicate possible suppression of ROS synthesis is also mirrored by early large increases in proline, quinate, γ -aminobutyric acid (GABA) and mannitol, which can all generate (either directly or indirectly) powerful ROS scavenging/anti-oxidant activity (Bouche and Fromm, 2004; Niggeweg *et al.*, 2004; Chen and Dickman, 2005; Solomon *et al.*, 2007) and are commonly associated with abiotic stress responses in plants. Additionally, the level of threonate (a by-product of ascorbate catabolism) also increased rapidly in *M. grisea*-infected host plants, which may be indicative of a large increase in ascorbate/dehydroascorbate anti-oxidant activity (Debolt *et al.*, 2007). When considered together, the overall changes in metabolism in susceptible interactions may negate rapid, localized production of ROS and block induction of plant defences.

Nutrient acquisition and fungal proliferation during rice blast infections

There is still considerable uncertainty with respect to which nutrients are derived directly from the host and which are synthesized *de novo* by the invading pathogen (Solomon *et al.*, 2003, 2007; Swarbrick *et al.*, 2006; Divon and Fluhr, 2007; Sutton *et al.*, 2007). It has been reported in susceptible barley-powdery mildew (Swarbrick *et al.*, 2006) and other susceptible host-pathogen interactions that invertase activity increases after infection, accompanied by progressive accumulation of hexoses and sucrose and a reduction in photosynthesis. Currently very little is known concerning substrate utilization and carbon source sequestration by *M. grisea* during growth in host leaves. Sucrose, glucose and fructose levels increased dramatically following appearance of visible lesions induced by *M. grisea*, which is indicative of infected leaves becoming significant sinks for photosynthate (Figure 5). However, we also found that levels of sucrose and aspartate (major carbon and nitrogen sources that are transported long distances), as well as alanine and the TCA cycle intermediates malate and citrate, had already increased approximately twofold in infected leaves by 48 h (see box plots in Figures 4a and 5a) in pre-symptomatic tissues. At this stage, invading fungal hyphae were still largely confined to the relatively small number of initially invaded epidermal cells (see Figure 6g). The timing and extent of these metabolic changes therefore suggest that the pathogen may be able to modulate metabolism and metabolite transport in distant mesophyll and vascular tissues while still colonizing the initial epidermal cell.

An increase in amino acids in pathogen-challenged leaves has been reported previously, predominantly in biotrophic fungal infections where no cell death occurs (Solomon *et al.*, 2003). It has been suggested that increases in methionine, arginine, and most likely tryptophan, cysteine, proline and histidine, are general features of pathogenesis, implying that these primary metabolites might be largely derived directly from plant cells (Solomon *et al.*, 2003). *Brachypodium* leaves infected with *M. grisea* show very high levels of glutamate, with glutamine levels two orders of magnitude lower (Figure 5a). An early increase in aspartate concentration was followed by an increase in pyruvate and TCA intermediates, and a parallel increase in the levels of amino acids derived from pyruvate (leucine, valine and alanine), α -ketoglutarate (glutamine) and aspartate (homoserine). Because glutamine derived from glutamate is the main nitrogen donor for amino acid synthesis, these data suggest that either glutamate, or conversion of translocated aspartate to glutamate, might provide a major source of nitrogen for protein synthesis in growing hyphae, rather than uptake of a range of amino acids from host tissues (Figure 5b). GABA also accumulates to similar levels as aspartate, and is also easily converted into glutamine, thus possibly providing an additional source of translocated nitrogen for the growing pathogen (Bouche and Fromm, 2004). It has been proposed recently that GABA may be a pivotal link between central metabolism of both carbon and nitrogen compounds (Fait *et al.*, 2007), and thus alterations in its metabolism in susceptible plants may have more far-reaching effects on the metabolome than a simple diversion from ROS production to nutrient source (Oliver and Solomon, 2004).

The rapid increase of glucose and fructose at day 4 and 5 was accompanied by a large increase in mannitol and more modest increases in glycerol and erythritol concentrations. Mannitol has been proposed previously as an important carbohydrate for fungal growth (Solomon *et al.*, 2007). Inducible hexose transporters have been described in many plant pathogens (Solomon *et al.*, 2003; Divon and Fluhr, 2007), and have been shown to be transcriptionally up-regulated in haustoria of the rust fungus *Uromyces fabae* (Voegelé *et al.*, 2001; Jakupovic *et al.*, 2006). As mannitol is membrane-impermeable, conversion of imported hexoses to mannitol might maintain a gradient for continued uptake and sequestration of photoassimilates. Continuous water influx is necessary for hyphal growth and turgor, which are required for invasive growth through living tissue (Kankanala *et al.*, 2007). Filamentous fungi control cytoplasmic osmotic pressure through ion accumulation and synthesis of compatible osmolytes, including sugar alcohols and glycerol (Kankanala *et al.*, 2007). Thus the dramatic increase in mannitol, glycerol and erythritol between days 3 and 4 could be associated with osmolyte production during the rapid increase in fungal biomass as the pathogen radiates

out of primary-infected epidermal cells. This pattern of metabolite accumulation is mirrored by a number of currently structurally uncharacterized GC-MS peaks (e.g. Figure S4) that may represent further key fungal metabolites required for plant colonization.

In summary, the data presented show a rapid and dynamic perturbation of host metabolism by *M. grisea* during plant infection that is conserved in three distinct host species. Although traditionally classified as a hemi-biotrophic fungal pathogen, the rice blast fungus appears to proliferate biotrophically during colonization of plant tissue, growing within living plant cells and travelling between cells by utilizing pit field sites (Kankanala *et al.*, 2007). Disease symptom formation occurs between 72 and 96 h after infection, and the necrotic lesions may be the result of de-repression of host defences, which appear to be actively suppressed during early fungal invasion. Although *M. grisea* is known to produce toxins, there is no direct evidence that these are deployed to kill plant cells during disease symptom development. Whether *M. grisea* undergoes necrotrophic growth is therefore still unknown, although it is likely that sporulation from disease lesions, which occurs 5–6 days after infection, is fuelled by nutrient release from dying host cells. Thus, the metabolic changes observed in our study are consistent with the biotrophic growth habit of *M. grisea* during plant tissue invasion, its suppression of host defences and its alteration of plant metabolic pathways to allow its growth in living plant cells. A detailed investigation of metabolic interactions between the host and invading pathogen during the first 24–48 h after infection may therefore reveal important targets for the fungal effector molecules that are responsible for disease progression.

EXPERIMENTAL PROCEDURES

Plant growth, infection and harvesting of tissues

All plants were fully susceptible to the Guy11 strain of *Magnaporthe grisea* (Routledge *et al.*, 2004). Seed sources, plant growth, infection and harvesting of leaf sections from plant genotypes *Brachypodium distachyon* ABR1, *Hordeum vulgare* Golden Promise and *Oryza sativa* CO39 have been described in detail previously (Parker *et al.*, 2008). The first harvest at 24 h post-inoculation corresponded to the end of a developmental phase involving spore germination, appressorium formation and epidermal cell penetration by the penetration peg. The second harvest at 48 h post-inoculation represented completion of the primary biotrophic interaction with the host, including development of bulbous invasive hyphae within the initially colonized epidermal cell. At the third harvest point (72 h), the fungus had spread to adjacent epidermal cells and underlying mesophyll cells. At this point, the first visible signs of disease had started to appear as small chlorotic lesions. At the fourth harvest, 96 h post-infection, visible necrotic lesions were evident. In our experiments, sporulation of the fungus from disease lesions was inhibited by maintaining lower humidity conditions to avoid a switch to reproductive development that might dominate or obscure metabolome changes in the host. The final harvest time point at 120 h post-infection with *M. grisea* represents the stage at

which fungal biomass begins to predominate in infected leaves. Leaf sections (4 cm) of each species (20 replicates, each from a different plant) were placed in 2 ml Eppendorf tubes each containing a 4 mm ball bearing, snap-frozen in liquid nitrogen, and stored at -80°C . All batches of infected plants were subjected to quality control as summarized in Figure S1 following metabolite fingerprinting by FIE-MS.

Histochemical staining to localize fungal hyphae and sites of ROS production

KOH/aniline blue staining of infected leaf segments viewed under UV epifluorescence illumination was used to visualize fungal hyphae as described by Hood and Shew (1996). *Brachypodium distachyon* leaves were excised at the base at specific time points following *M. grisea* infection and immersed immediately in 3,3-diaminobenzidine tetrahydrochloride (DAB) solution (1.0 mg/ml, pH 3.8) for 24 h. ROS accumulation (orange-brown staining) was observed under a light microscope after de-staining with 96% v/v ethanol for 1 h at 50°C as described by Thordal-Christensen *et al.* (1997).

Sample preparation for metabolome analysis

The sample extraction process involved the use of a single-phase solvent (chloroform/methanol/water) that has been optimized for recovery of a wide range of metabolites, offering relatively comprehensive coverage of the metabolome (Catchpole *et al.*, 2005; Liseč *et al.*, 2006; Beckmann *et al.*, 2007). Milling in a Retsch Mixer Mill, MM200 (Retsch, <http://www.retsch.com/>) (30 sec at 30 Hz) and extraction of plant tissues for metabolome analysis in a chilled solvent (CHCl_3 :MeOH:H₂O 1:2.5:1 v/v/v, at approximately -18°C) has been described previously (Parker *et al.*, 2008). Following centrifugation (18 000 g for 3 min at 0°C), the resulting supernatant was removed in three portions: 100 μl was removed for metabolite fingerprinting by FIE-MS, 100 μl was removed and dried *in vacuo* for derivatization prior to GC-MS analysis, and the remainder was stored in a liquid state at -80°C .

Flow infusion electrospray mass spectrometry analysis

Samples were randomized, and 20 μl was injected using a Surveyor HPLC system into a mobile phase of methanol:water (50:50 v/v; flow rate 60 $\mu\text{l}/\text{min}$), and an FIE-MS fingerprint was generated on a LTQ linear ion trap mass spectrometer (ThermoFinnigan, <http://www.thermo.com/>) in positive and negative mode as described previously (Beckmann *et al.*, 2007, 2008). Ion intensities were detected in the scan range between m/z 50 and 2000, and whole infusion profiles were electronically binned to 1 atomic mass unit (amu) between -0.3 amu and $+0.7$ amu. Mass spectra were combined in a single intensity matrix (runs \times m/z ratios) for each ion mode. Each run was log-transformed and normalized to the total ion count for statistical analysis. Only mass bins between 110 and 1100 amu were kept for data analysis. Ionization products (m/z) highlighted as significant ($P \leq 0.001$) after data mining were annotated using the ARMeC database (Overy *et al.*, 2008; <http://www.armac.org/>) as described previously (Beckmann *et al.*, 2007). As several overlapping solutions predicting the presence of different metabolites were often possible, the most likely combination of ions putatively identifying a specific metabolite were confirmed (where signal intensity allowed) by MS/MSⁿ experiments (Overy *et al.*, 2008).

GC-TOF-MS analysis

GC-TOF-MS analysis was performed as described previously (Catchpole *et al.*, 2005; Liseč *et al.*, 2006; Beckmann *et al.*, 2007) using tetramethylsilane derivatization and a Pegasus III GC-TOF-MS

system (Leco Inc., <http://www.leco.com/>) fitted with a 20 m DB5 MS column. Peak finding and peak de-convolution were performed using ChromaTof software (Leco Inc.). Mass spectra of all detected compounds were compared with spectra in National Institute of Standards and Technology library, and with in-house and publicly available databases. Targeted peak lists were generated, and the peak apex intensity of a characteristic mass in a retention time window for each GC-MS data set (using Matlab) was saved in the form of an intensity matrix (run \times metabolite) for further statistical analysis.

Data analysis

Supervised multivariate classification tools, including linear discriminant analysis (LDA) and random forest (RF) decision trees, were used as reported previously to define when major changes in the metabolome occurred during fungal infection of host plants (Enot *et al.*, 2006, 2007, 2008; Enot and Draper, 2007). A range of feature-ranking methods were used subsequently to identify *m/z* signals common to all three host species that altered significantly ($P \leq 0.001$) on each day after infection (Enot *et al.*, 2007, 2008). Linear discriminant analysis was performed with the *nlda* function implemented using the *FIEmspro* package (Enot *et al.*, 2008). For both RF and LDA, the 'leave one out' strategy was adopted to assess model predictive accuracies. The statistical significance of the importance score and model margins were assessed by permutation testing. One thousand random re-orderings of the class labels were used to estimate the permutation-based *P* values. Univariate correlation analysis of individual signals was performed using variables that fell below a specified threshold in at least one of the comparisons. The absolute value of the correlation coefficient between variables was used as the similarity measure for performing hierarchical cluster analysis with the complete linkage as the clustering method (*hclust* function in R).

Statistical calculations were performed using R (R 2.4.) and Matlab (version 6.5 R13SP1, <http://cran.r-project.org/>) on a PowerPC G5 (dual 1.8 GHz, 2 GB SDRAM) as described previously (Enot *et al.*, 2006, 2007, 2008). Briefly, principal component analysis and eigenvalue decomposition were performed on the co-variance matrix using the mean-centred matrix and the *princomp* Matlab function. Random forest analysis was performed using the R package *randomForest* with defaults settings, except that the number of trees was set to 1000.

Analysis of NADP-malic enzyme activity

For *in situ* NADP-ME activity assays, *B. distachyon* seedlings were fixed in 2% w/v paraformaldehyde and 1 mM dithiothreitol in PBS pH 7.0 (0.1% w/v Na₂HPO₄, 0.03% w/v NaH₂PO₄ and 0.9% w/v NaCl) at 4°C for 1 h, and then rinsed overnight in de-ionized water at 4°C to remove soluble carbohydrates (Sergeeva *et al.*, 2004). Fixed plants were stained for NADP-ME activity by submerging the seedlings in a staining solution containing 50 mM Tris/HCl pH 7.5, 10 mM L-malate, 10 mM MgCl₂, 0.5 mM NADP, 35 µg/ml nitroblue tetrazolium and 0.85 µg/ml phenazine methosulfate for 3 h at 30°C in a water bath, followed by 1 h de-staining in 96% v/v ethanol at 50°C (Wheeler *et al.*, 2005).

NADP-ME activity was measured in crude extracts (three replicates) of *B. distachyon* produced by harvesting 30–40 mg of pooled leaf samples (5 \times 4 cm sections) at appropriate times after fungal or mock inoculation (gelatine/water) and snap freezing in liquid nitrogen. Frozen tissue was homogenized in 200 µl of extraction buffer containing 100 mM Tris/HCl pH 7.5, 5 mM MgCl₂, 2 mM EDTA, 10% v/v glycerol, 10 mM 2-mercaptoethanol and 1 mM phenylmethylsulfonyl fluoride (PMSF) using a pre-chilled Retsch Mixer Mill, MM200 (45 sec at 30 Hz). The extracted samples were centrifuged at 10 000 g for 15 min, and supernatants were used for either

NADP-ME activity measurements by spectrophotometry (Liu *et al.*, 2007) or subjected to native PAGE for in-gel NADP-ME activity measurements as described by Wheeler *et al.* (2005).

ACKNOWLEDGEMENTS

We would like to thank Rob Darby for maintaining laboratory infrastructure and Emily Duval for assisting with sample extraction and mass spectrometry. Metabolite analysis, statistical work and biological materials were performed and materials generated with funding from the UK Biotechnology and Biological Sciences Research Council grants BB/D006953/1 and BB/D006791/1 awarded to J.D. and N.J.T.

SUPPORTING INFORMATION

Additional Supporting Information may be found in the online version of this article:

Figure S1. Use of linear discriminant analysis (LDA) to validate sample class alignment in data derived from FIE-MS fingerprint analysis of various batches of pathogen-challenged plants.

Figure S2. Areas of metabolism that alter during disease establishment as suggested by FIE-MS fingerprinting (negative ion data).

Figure S3. GC-TOF-MS analysis of samples representing disease progression in *M. grisea* infection of *B. distachyon* ABR1.

Figure S4. Unknown metabolites with high discriminatory power between various phases of disease progression.

Figure S5. Comparison of discriminatory metabolite behaviour in four susceptible hosts.

Figure S6. Grading scale to monitor relative levels of ROS by DAB staining at sites of fungal infection.

Figure S7. Spatial relationships between visible lesions, fungal hyphae and *in situ* NADP-ME activity in susceptible *B. distachyon* (ABR1) leaves infected by *M. grisea*.

Figure S8. NADP-ME transcription during pathogen challenge in rice leaves infected by *M. grisea*.

Table S1. Distance measures and numbers of potentially explanatory features in random forest models comparing metabolome changes at consecutive phases of disease progression in *B. distachyon* ABR1 infected with *M. grisea*.

Table S2. Positive ion FIE-MS signal putative annotations derived from ARMeC.

Table S3. Negative ion FIE-MS signal putative annotations derived from ARMeC.

Please note: Wiley-Blackwell are not responsible for the content or functionality of any supporting materials supplied by the authors. Any queries (other than missing material) should be directed to the corresponding author for the article.

REFERENCES

- Allan, A.C. and Fluhr, R. (1997) Two distinct sources of elicited reactive oxygen species in tobacco epidermal cells. *Plant Cell*, **9**, 1559–1572.
- Allwood, J.W., Ellis, D.I., Heald, J.K., Goodacre, R. and Mur, L.A. (2006) Metabolomic approaches reveal that phosphatidic and phosphatidyl glycerol phospholipids are major discriminatory non-polar metabolites in responses by *Brachypodium distachyon* to challenge by *Magnaporthe grisea*. *Plant J.* **46**, 351–368.
- Beckmann, M., Enot, D.P., Overy, D.P. and Draper, J. (2007) Representation, comparison, and interpretation of metabolome fingerprint data for total composition analysis and quality trait investigation in potato cultivars. *J. Agric. Food. Chem.* **55**, 3444–3451.
- Beckmann, M., Parker, D., Enot, D., Duval, E. and Draper, J. (2008) High throughput metabolome fingerprinting using flow injection electrospray mass spectrometry. *Nat. Protoc.* **3**, 486–504.
- Bino, R.J., Hall, R.D., Fiehn, O. *et al.* (2004) Potential of metabolomics as a functional genomics tool. *Trends Plant Sci.* **9**, 418–425.

- Both, M., Csukai, M., Stumpf, M.P.H. and Spanu, P.D. (2005) Gene expression profiles of *Blumeria graminis* indicate dynamic changes to primary metabolism during development of an obligate biotrophic pathogen. *Plant Cell*, **17**, 2107–2122.
- Bouche, N. and Fromm, H. (2004) GABA in plants: just a metabolite? *Trends Plant Sci.* **9**, 110–115.
- Caldo, R.A., Nettleton, D. and Wise, R.P. (2004) Interaction-dependent gene expression in Mla-specified response to barley powdery mildew. *Plant Cell*, **16**, 2514–2528.
- Casati, P., Drincovich, M.F., Edwards, G.E. and Andreo, C.S. (1999) Malate metabolism by NADP-malic enzyme in plant defense. *Photosynth. Res.*, **61**, 99–105.
- Catchpole, G., Beckmann, M., Enot, D.P. et al. (2005) Hierarchical metabolomics demonstrates substantial compositional similarity between genetically modified and conventional potato crops. *Proc. Natl Acad. Sci. USA*, **4**, 14458–14462.
- Chen, C.B. and Dickman, M.B. (2005) Proline suppresses apoptosis in the fungal pathogen *Colletotrichum trifolii*. *Proc. Natl Acad. Sci. USA*, **102**, 3459–3464.
- Chisholm, S.T., Coaker, G., Day, B. and Staskawicz, B.J. (2006) Host–microbe interactions: shaping the evolution of the plant immune response. *Cell*, **124**, 803–814.
- Chou, H.-M., Bundock, N., Rolf, S.A. and Scholes, J.D. (2000) Infection of *Arabidopsis thaliana* leaves with *Albugo candida* (white blister rust) causes a reprogramming of host metabolism. *Mol. Plant Pathol.* **1**, 99–113.
- Debolt, S., Melino, V. and Ford, C.M. (2007) Ascorbate as a biosynthetic precursor in plants. *Ann. Bot.* **99**, 3–8.
- Divon, H.H. and Fluhr, R. (2007) Nutrition acquisition strategies during fungal infection of plants. *FEMS Microbiol. Lett.* **266**, 65–74.
- Doehlemann, G., Wahl, R., Horst, R.J. et al. (2008) Reprogramming a maize plant: transcriptional and metabolic changes induced by the fungal biotroph *Ustilago maydis*. *Plant J.* **56**, 181–195.
- Draper, J., Mur, L.A., Jenkins, G., Ghosh-Biswas, G.C., Bablak, P., Hasterok, R. and Routledge, A.P. (2001) *Brachypodium distachyon*. A new model system for functional genomics in grasses. *Plant Physiol.* **127**, 1539–1555.
- Egan, M.J., Jones, M.A., Smirnov, N., Wang, Z.Y. and Talbot, N.J. (2007) Generation of reactive oxygen species by fungal NADPH oxidases is required for rice blast disease. *Proc. Natl Acad. Sci. USA*, **104**, 11772–11777.
- Enot, D.P. and Draper, J. (2007) Statistical measures for validating plant genotype similarity assessments following multivariate analysis of metabolome fingerprint data. *Metabolomics*, **3**, 349–355.
- Enot, D.P., Beckmann, M., Overy, D. and Draper, J. (2006) Predicting interpretability of metabolome models based on behavior, putative identity, and biological relevance of explanatory signals. *Proc. Natl Acad. Sci. USA*, **103**, 14865–14870.
- Enot, D.P., Beckmann, M. and Draper, J. (2007) Detecting a difference – assessing generalisability when modelling metabolome fingerprint data in longer term studies of genetically modified plants. *Metabolomics*, **3**, 335–347.
- Enot, D.P., Lin, W., Beckmann, M., Parker, D., Overy, D.P. and Draper, J. (2008) Pre-processing, classification modelling and feature selection using flow injection electrospray mass spectrometry (FIE-MS) metabolome fingerprint data. *Nat. Protoc.* **3**, 446–470.
- Fait, A., Fromm, H., Walter, D., Galili, G. and Fernie, A.R. (2007) Highway or byway: the metabolic role of the GABA shunt in plants. *Trends Plant Sci.* **13**, 14–19.
- Herrmann, K.M. and Weaver, L.M. (1999) The shikimate pathway. *Annu. Rev. Plant Physiol. Plant Mol. Biol.* **50**, 473–503.
- Hood, M.E. and Shew, H.D. (1996) Application of KOH-aniline blue fluorescence in the study of plant fungal interactions. *Phytopathology*, **86**, 704–708.
- Huckelhoven, R. (2007) Cell wall-associated mechanisms of disease resistance and susceptibility. *Annu. Rev. Phytopathol.* **45**, 101–127.
- Jakupovic, M., Heintz, M., Reichmann, P., Mendgen, K. and Hahn, M. (2006) Microarray analysis of expressed sequence tags from haustoria of the rust fungus *Uromyces fabae*. *Fungal Genet. Biol.*, **43**, 8–19.
- Jantasuriyarat, C., Gowda, M., Haller, K. et al. (2005) Large-scale identification of expressed sequence tags involved in rice and rice blast fungus interaction. *Plant Physiol.* **138**, 105–115.
- Kankanala, P., Czymbek, K. and Valent, B. (2007) Roles for rice membrane dynamics and plasmodesmata during biotrophic invasion by the blast fungus. *Plant Cell*, **19**, 706–724.
- Kawasaki, T., Koita, H., Nakatsubo, T., Hasegawa, K., Wakabayashi, K., Takahashi, H., Urnemura, K., Urnezawa, T. and Shimamoto, K. (2006) Cinnamoyl-CoA reductase, a key enzyme in lignin biosynthesis, is an effector of small GTPase Rac in defense signaling in rice. *Proc. Natl Acad. Sci. USA*, **103**, 230–235.
- Lisec, J., Schauer, N., Kopka, J., Willmitzer, L. and Fernie, A.R. (2006) Gas chromatography mass spectrometry-based metabolite profiling in plants. *Nat. Protoc.* **1**, 387–396.
- Liu, S., Cheng, Y., Zhang, X., Guan, Q., Nishiuch, S., Hase, K. and Takano, T. (2007) Expression of an NADP-malic enzyme gene in rice (*Oryza sativa* L.) is induced by environmental stresses; over-expression of the gene in *Arabidopsis* confers salt and osmotic stress tolerance. *Plant Mol. Biol.* **64**, 49–58.
- Niggeweg, R., Michael, A.J. and Martin, C. (2004) Engineering plants with increased levels of the antioxidant chlorogenic acid. *Nat. Biotechnol.* **22**, 746–754.
- Oliver, R.P. and Solomon, P.S. (2004) Does the oxidative stress used by plants for defence provide a source of nutrients for pathogenic fungi? *Trends Plant Sci.* **9**, 472–473.
- Overy, D.P., Enot, D.P., Tailliar, K., Jenkins, H., Parker, D., Beckmann, M. and Draper, J. (2008) Explanatory signal interpretation and metabolite identification strategies for nominal mass FIE-MS metabolite fingerprints. *Nat. Protoc.* **3**, 471–485.
- Parker, D., Beckmann, M., Enot, D., Overy, D., Caracuel-Rios, Z., Gilbert, M., Talbot, N. and Draper, J. (2008) Rice blast infection of *Brachypodium distachyon* as a model system to study dynamic host/pathogen interactions. *Nat. Protoc.* **3**, 435–445.
- Routledge, A., Shelley, G., Smith, J., Talbot, N., Draper, J. and Mur, L. (2004) *Magnaporthe grisea* interactions with the model grass *Brachypodium distachyon* closely resemble those with rice (*Oryza sativa*). *Mol. Plant Pathol.* **5**, 254–265.
- Schaaf, J., Walter, M.H. and Hess, D. (1995) Primary metabolism in plant defense – regulation of a bean malic enzyme gene promoter in transgenic tobacco by developmental and environmental cues. *Plant Physiol.* **108**, 949–960.
- Sergeeva, L.I., Vonk, J., Keurentjes, J.J.B., van der Plas, L.H.W., Koornneef, M. and Vreugdenhil, D. (2004) Histochemical analysis reveals organ-specific quantitative trait loci for enzyme activities in *Arabidopsis*. *Plant Physiol.* **134**, 1–9.
- Singh, S.A. and Christendat, D. (2006) Structure of *Arabidopsis* dehydroquinase dehydratase–shikimate dehydrogenase and implications for metabolic channelling in the shikimate pathway. *Biochemistry*, **45**, 7787–7796.
- Solomon, P.S., Tan, K.-C. and Oliver, R.P. (2003) The nutrient supply of pathogenic fungi; a fertile field for study. *Mol. Plant Pathol.* **4**, 203–210.
- Solomon, P.S., Waters, O.D.C. and Oliver, R.P. (2007) Decoding the mannitol enigma in filamentous fungi. *Trends Microbiol.* **15**, 257–262.
- Sutton, P.N., Gilbert, M.J., Williams, L.E. and Hall, J.L. (2007) Powdery mildew infection of wheat leaves changes host solute transport and invertase activity. *Physiol. Plant.* **129**, 787–795.
- Swarbrick, P., Schulze-Lefert, P. and Scholes, J. (2006) Metabolic consequences of susceptibility and resistance (race-specific and broad spectrum) in barley leaves challenged with powdery mildew. *Plant Cell Environ.* **29**, 1061–1076.
- Talbot, N.J. (2003) On the trail of a cereal killer: exploring the biology of *Magnaporthe grisea*. *Annu. Rev. Microbiol.* **57**, 177–202.
- Thordal-Christensen, H., Zhang, Z., Wei, Y. and Collinge, D.B. (1997) Subcellular localization of H₂O₂ in plants. H₂O₂ accumulation in papillae and hypersensitive response during the barley–powdery mildew interaction. *Plant J.* **11**, 1187–1194.
- Torres, M.A., Jones, J.D.G. and Dangl, J.L. (2006) Reactive oxygen species signalling in response to pathogens. *Plant Physiol.* **141**, 373–378.
- Voegele, R.T., Struck, C., Hahn, M. and Mendgen, K. (2001) The role of haustoria in sugar supply during infection of broad bean by the rust fungus *Uromyces fabae*. *Proc. Natl Acad. Sci. USA*, **98**, 8133–8138.
- Walters, D. (2003) Resistance to plant pathogens: possible roles for free polyamines and polyamine catabolism. *New Phytol.* **159**, 109–115.
- Wheeler, M.C.G., Tronconi, M.A., Drincovich, M.F., Andreo, C.S., Flugge, U. and Maurino, V. (2005) A comprehensive analysis of the NADP-malic enzyme gene family of *Arabidopsis*. *Plant Physiol.* **139**, 39–51.
- Yoda, H., Yamaguchi, Y. and Sano, H. (2003) Induction of hypersensitive cell death by hydrogen peroxide produced through polyamine degradation in tobacco plants. *Plant Physiol.* **132**, 1973–1981.